Available online at www.sciencedirect.com

ScienceDirect

Procedia Engineering 126 (2015) 163 – 168

Procedia Engineering

www.elsevier.com/locate/procedia

7th International Conference on Fluid Mechanics, ICFM7

Numerical investigation of hypersonic unsteady flow around a spiked blunt-body

Yu Ma*, Xiaowei Liu, Ping Ou

China Academy of Aerospace Aerodynamiscs, Beijing, China

Abstract

The obvious unsteady flow characteristics of the flow field around the spiked blunt-body have negative effect on the drag reduction of vehicle and the thermo-protection of the head. The hypersonic self-sustained oscillatory flow was numerical simulated, and the flow structure and mechanism of the three process of one cycle: collapse, inflation and withhold, were discussed in detail. The correspondence between the drag coefficient curve and the different flow structure was obtained, which will provide basis to the drag reduction and thermo-protection of hypersonic blunt-body vehicle through flow control in the future.

Peer-review under responsibility of The Chinese Society of Theoretical and Applied Mechanics (CSTAM)

Keywords: Hypersonic, Unsteady, Aerospike

1. Introduction

Aerospikes are aerodynamic devices for rockets, missiles, and reentry vehicles. Separated flow formed around the aerospike reduces the wave drag and heat-transfer rates on the nose surface of vehicles in supersonic and hypersonic flight conditions. Several application cases of aerospikes exist already. The M-3S-II rocket, the Japanese solid booster, has fixed aerospikes at the top of its two strap-on boosters to reduce atmospheric drag during its ascent. Tridents I and II are spike-nosed submarine-launched ballistic missiles.

The separation flow around the aerospike is essentially unstable. Therefore, many researchers have reported on its aerodynamic characteristics. In the early 1950s, Robins[1] conducted an investigation to determine the effect of

* Corresponding author. Tel.: +86-10-885-36342; fax: +86-10-683-74758.
E-mail address: universema@126.com

Peer-review under responsibility of The Chinese Society of Theoretical and Applied Mechanics (CSTAM)
doi:10.1016/j.proeng.2015.11.204

several seeker-nose configurations (cone spike, plain spike, slotted cone, spherical, conical, and parabolic) on the static longitudinal stability, the canard control characteristics, and lift and drag of a canard-type ramjet missile. Kubota et al.[2] also studied the feasibility of using spikes as drag and heat-transfer rate reducing devices on blunt bodies at hypersonic speeds. Mikhail[3,4] investigated dual flow modes of spike-nosed projectile configurations, pointing out that flow oscillation between the high-drag mode and the low-drag mode causes a buzzing phenomenon. In later studies, he conducted numerical simulations of the spike-nosed projectile with a tripping ring at the spike tip for preventing a high-drag mode. Feszty et al.[5,6] reported the driving mechanism of two distinct spike-induced unsteady flow modes: oscillation and pulsation. The oscillation flow mode is characterized by the foreshock shape change between a convex shape and a concave one, whereas the shock system changes dramatically in the pulsation flow mode. The oscillation mode is typical of longer spike lengths (L/D=1.5–2.5) and the pulsation mode of shorter ones (L/D=0.2–1.5).

Because of the difficulty of obtaining data from the flowfield at the high-speed freestreams considered (typically between Mach 2 and 10) and the high frequency of the events (1000–7500 Hz), the objective of the present work was therefore to use Fluent software as a tool for the detailed investigation of the driving mechanisms of high-speed unsteady spiked body flows, as well as the drag characteristic variation.

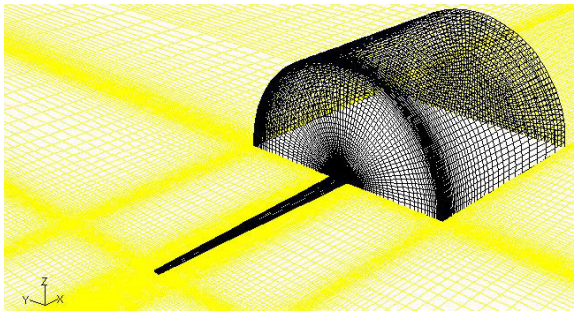

Fig. 1 The model and adapted grid

2. Numerical methods and computational grid

The model geometry was a forward-facing cylinder equipped with an aerospike of the length of *L/D* =1.00 (Fig. 1). The diameter of the cylinder is 60mm and the length is 55mm. The diameter of the windward of the aerospike is 0.025D and the other side is 0.07D.

Numerical simulation of flow field was done by commercial software *Fluent*. The two-equation RNG κ-ε turbulence mode was employed in this calculation, and the second order upwind Roe-FDS scheme was implemented for shock capturing. The fluid is ideal gas and boundary of the flow field is pressure-far field. The Mach number is 5. Steady-state calculations proceed in two phases: the freestream starting solution is initially smoothed using an explicit scheme, and then an implicit scheme is employed to obtain rapid convergence.

The hexahedral grid systems were generated with the computer code *Gambit*, which is distributed along with *Fluent*. The initial point of the fluid domain for computing is near to the aerospike because of the hypersonic flow. The computation domain is 1/4 of the actual axisymmetric flow field. A local refinement was adopted based on the flow field characteristic. The grid number is about 0.6 million, as show in Fig. 1.

3. Results and discussion

3.1. Self-sustained oscillatory flows

Unsteady spiked body flows can be put into context as a type of self-sustained oscillatory flows, according to the definition of Rockwell and Naudascher. These highly organized oscillatory flows, which include instabilities such as cavity flows, jet-edge, jet cylinder or jet-flap interactions etc., are sustained through a series of interacting events. Based on the investigation of Feszty, the pulsation phenomenon should appear for L/D=1 at present paper. The simulation results show that there are three processes in one cycle: collapse, inflation and withhold. The differences

in some details between the Feszty investigation and this paper are due to the Mach number and the aerospike nose shape dissimilarity. The unsteady spiked body flows bring about the big amplitude fluctuation of the drag coefficient curve, as shown in Fig. 2.

The abscissa of the Fig. 2 is no-dimensional time $t^*=t*U_\infty/D$, and the ordinate is drag coefficient C_D. The horizontal line denotes the time average value of C_D. The sequence of 24 flow-visualization frames is shown in Fig. 3-Fig.8, and the nondimensional time difference between each of these frames was $\Delta t^* =0.224$.

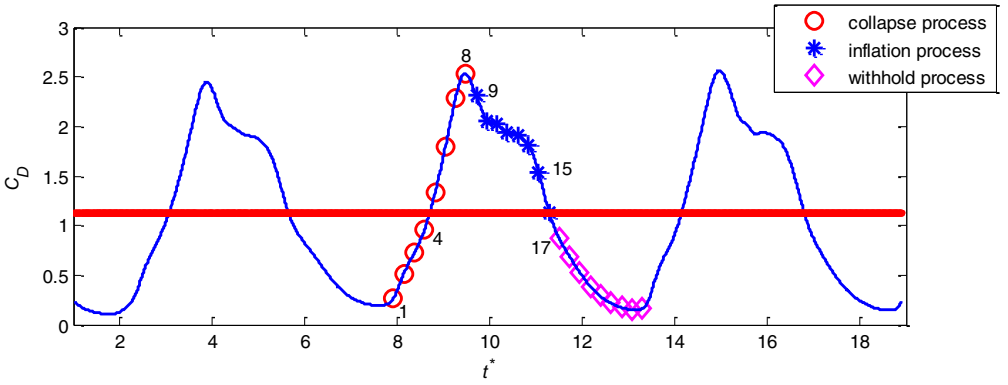

Fig. 2 The model drag coefficient history

3.2. Collapse process

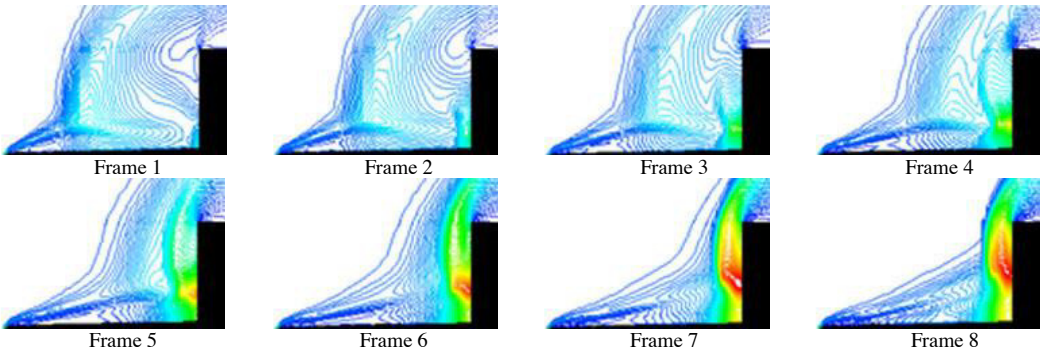

Fig. 3 destiny isoline variety in collapse process

The destiny isoline varieties in collapse process are shown in Fig. 3. Because of the numerous flow features emerging and dispersing during these events, flow schematics helping their identification were created in Fig. 4, Fig. 6 and Fig. 8 in which shock waves were noted as W, separated regions as P, shear layers as L, and vortical regions as V. They were numbered in the order of their appearance during the pulsation cycle.

In frame 1 (Fig. 3) bow wave W2 (Fig. 4) has already accomplished its expansion and starts to migrate toward the afterbody. As the most forward portion of the aerospike becomes exposed to supersonic freestream, an oblique conical foreshock W1 will emanate from the aerospike tip. The flow behind W1 is supersonic and is decelerated through another oblique shock wave W3, emanating from the triple point T1. As this oblique wave interacts with the boundary layer on the aerospike, a separated region P1 is formed. By frame 2 separation region P1 has grown downstream, tracking the collapsing bow wave. P2, on the other hand, has moved farther forward ahead of the growing bow wave W5, generating a weak oblique shockW4. As W4 intersects W5, another triple shock system similar to the one at the aerospike tip is formed (T2, W6). With the developing of the flowfield, a significant vortical region V1 is formed, as shown in Fig. 4a.

With the elapse of time, the collapsing bow wave move downstream, the new bow wave move upstream, and at last the two bow waves merge. In frames 7 and 8 the two separated regions P1 and P2 gradually grow and the drag

coefficient reach the most value at the same time, as shown in Fig. 4b.

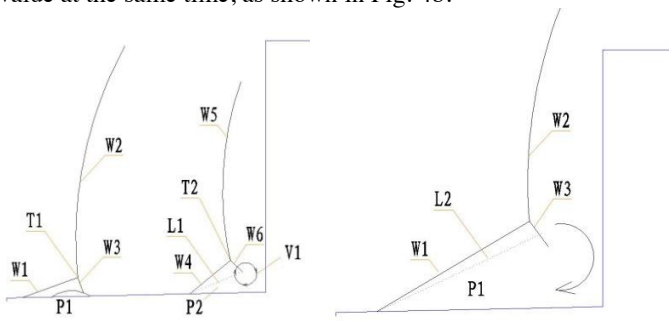

a) based on frames 3 and 4 b) based on frame 8

Fig. 4 Scheme of the shock system during collapse

3.3. Inflation process

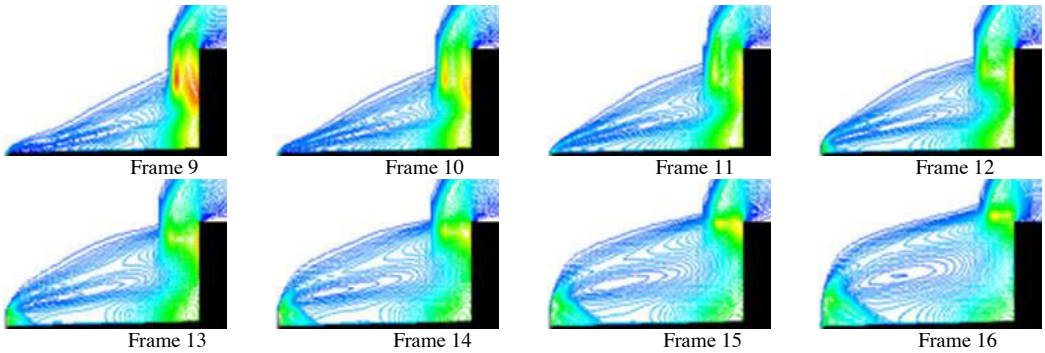

Fig. 5 destiny isoline variety in inflation process

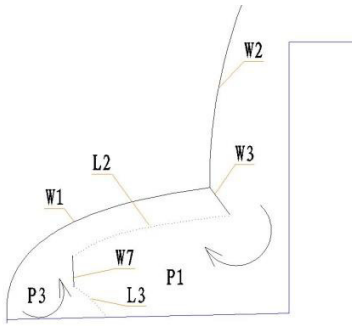

Fig. 6 Scheme of the shock system during inflation (based on frames 13 and 14)

The destiny isoline varieties in inflation process are shown in Fig. 5. The pressure and destiny after shock wave bow W2 reach their maximum at first of inflation process. The pressure field of the residual of vortical region V1 starts to enlarge and weaken as the high-pressure gas accumulated at the cylinder face escapes upstream with supersonic speeds. The shock wave W1 turns to a curve line at the same time. By frames 10 separation point P1 reaches the aerospike tip, and the recirculation zone starts to expand laterally. This will make the angle of foreshock W1 near the aerospike tip grow, and yield an increase in the pressure behind the shock so the recirculated supersonic flow has to be decelerated to these conditions before reentering shear layer L2. Hence, an internal normal bow wave W7 is generated in the vicinity of the aerospike tip shoulder (frames 11 and 12 and also Fig. 6), and as it interacts with the boundary layer yet another separation P3; embedded in the recirculation zone, occurs. Frame 12 marks the

first time instant of foreshock W1 becoming normal near the center line as it detaches from the aerospike tip. This means the creation of a sizeable high-pressure region behind this bow wave, causing shear layer L2 to be lifted off from the aerospike tip. As shear layer L2 moves away from the center, the triple point is gradually displaced in the lateral direction. By frames 13-16, the more flow becomes involved in this process, the larger the normal portion of the foreshock becomes.

3.4. Withhold process

The destiny isoline varieties in withhold process are shown in Fig. 7. During this process, shock W1 transforms from a combined normal and oblique shock to a predominantly normal bow wave W2. With the liftoff of the shock system, a new oblique shock W1 emerges from the tip of the aerospike (frame 17), and becomes more and more visible (frames 18-21). A new shock system comes into being, as shown in Fig. 8. The flow behind W1 is supersonic and is decelerated through another oblique shock wave W3, and a new separated region P4 is formed after the W1.

At the last time of the withhold process, the drag coefficient reaches its minimum, as shown in Fig. 2. With the oblique shock W1 separating from the aerospike tip, the new shock system move downstream rapidly and a new flow cycle begins.

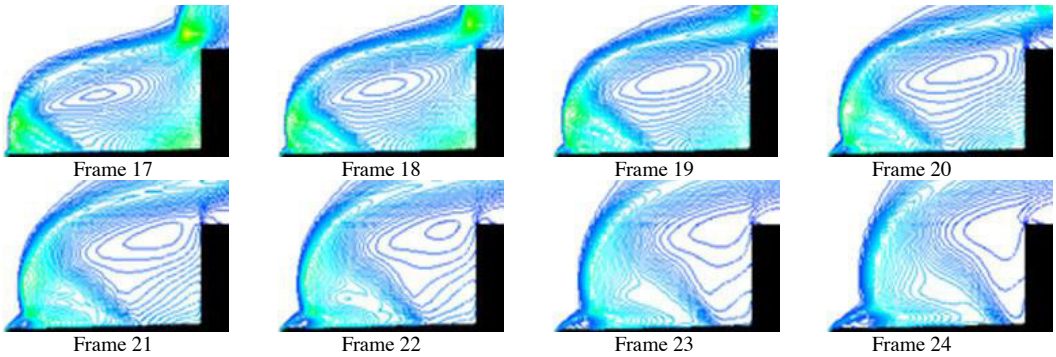

Fig. 7 destiny isoline variety in withhold process

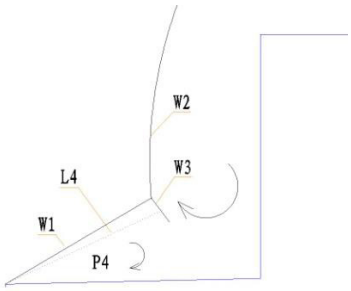

Fig. 8 Scheme of the shock system during withhold (based on frames 20 and 24)

4. Conclusions

The correspondence between the drag coefficient curve and the different flow structure was obtained through the investigation of present paper. The collapse process is corresponding to the increasing process of the drag cure, and the maximum value appears at the end of the collapse process. The inflation and withhold processes are corresponding to the decreasing process of the drag cure, and the minimum value appears at the end of the withhold process. Some characteristics of the flow around the blunt aerospike have been obtained through this paper. The hypersonic oblique shock wave is very near to the shear layer from the aerospike, easily moving downstream in collapse process, and emerging earlier in withhold process, compared with the supersonic flow.

References

[1] Robins, A. W., "Preliminary Investigation of the Effects of Several Seeker-Nose Configurations on the Longitudinal Characteristics of a Canard-Type Missile at a Mach Number of 1.60," NACA RM-L53I18, 1953.
[2] Kubota, H., Watanuki, T., Matsumoto, S., Fujita, M., and Fukui, T., "Effect of Spike Attached on a Hemisphere in Hypersonic Flow," Proceedings of the 19th International Symposium on Space Technology and Science, edited by Motoki Hinada, The Japan Society for Aeronautical and Space Science, Tokyo, 1994, pp. 460–467.
[3] Mikhail, A. G., "Spike-Nosed Projectiles: Computations and Dual Flow Modes in Supersonic Flight," Journal of Spacecraft and Rockets, Vol. 28, No. 4, 1991, pp. 418–424.
[4] Mikhail, A. G., "Spike-Nosed Projectiles with Vortex Rings: Steady and Nonsteady Flow Simulations," Journal of Spacecraft and Rockets, Vol. 33, No. 1, 1996, pp. 8–14
[5] Feszty, D., Badcock, K. J., and Richards, B. E., "Driving Mechanism of High-Speed Unsteady Spiked Body Flows, Part 1: Pulsation Mode," AIAA Journal, Vol. 42, No. 1, 2004, pp. 95–106.
[6] Feszty, D., Badcock, K. J., and Richards, B. E., "Driving Mechanism of High-Speed Unsteady Spiked Body Flows, Part 2: Oscillation Mode," AIAA Journal, Vol. 42, No. 1, 2004, pp. 107–113.